Hindawi Publishing Corporation
Journal of Nanomaterials
Volume 2014, Article ID 358312, 9 pages
http://dx.doi.org/10.1155/2014/358312

Research Article

Effects of Surfactants on High Regularity of 3D Porous Nickel for Zn^{2+} Adsorption Application

Xiaogang Guo,[1] Xueming Li,[1] Yonghong Zheng,[2] Chuan Lai,[1] Wulin Li,[1] Binbin Luo,[1] and Daixiong Zhang[1]

[1] *College of Chemistry and Chemical Engineering, Chongqing University, No. 174, Shazhengjie, Shapingba District, Chongqing 400044, China*
[2] *Chongqing Fiber Inspection Bureau, No. 5, Yunshan North Road, Gaoxin Park, Beibu New District, Chongqing 401121, China*

Correspondence should be addressed to Xueming Li; lixuemingcqu@126.com

Received 23 November 2013; Revised 13 January 2014; Accepted 15 January 2014; Published 18 March 2014

Academic Editor: Fan Dong

Three-dimensional porous nickel (3D-PN) film with large specific surface area (A_s) and high porosity has been successfully prepared by hydrogen bubble dynamic template (HBDT) method. This work presents the effects of PEG 10000 and 1,4-butynediol as new additive combination on surface morphology of the PN film. Meanwhile, the application of 3D-PN in Zn^{2+} adsorption was preliminarily investigated in the paper. The surface area is determined as large as 166.7 cm^2/mg and the porosity is 0.762 when the concentration of PEG 10000 and 1,4-butynediol was 0.3 g/100 mL and 0.1 g/100 mL, respectively. The adsorption capacity (Q_t and Q (%)) of PN for Zn^{2+} is observed to be 9.145 mg/g and 0.691 for $Zn(NO_3)_2{\cdot}6H_2O$. The morphology and the microstructure, the product formation, the A_s the concentration of the metal ions were characterized by scanning electron microscopy (SEM), X-ray powder diffraction (XRD), electrochemical impedance spectroscopy (EIS), and atomic absorption spectrometry (AAS), respectively.

1. Introduction

Three-dimensional (3D) porous metals (Ni, Cu, Sn, etc.) [1–4], with highly porous dendritic walls and numerous nanoparticles, are considered as promising nanomaterials due to their importance to both academic study and technological applications in separation systems [5], sensors [6, 7], fuel batteries [8, 9], electrochemistry [10, 11], electronic materials [12], and high performance supercapacitors [13]. Many researchers have successfully developed the 3D porous metal films electrode materials by template-directed synthesis method. And commonly used templates are considered such as liquid crystal, high internal phase emulsion (HIPE), photonic crystals, porous polycarbonate membranes [14, 15], anodic alumina membranes [16], colloidal crystals [17], and echinoid skeletal structures [18]. Compared with other approaches, hydrogen bubble dynamic template (HBDT) with hydrogen bubbles as the template on the cathode at high current densities is the green and promising one with lots of advantages: low-cost equipment, controllable structure, facile one-step synthesis process, and easy elimination of the template [11, 19].

Recently, many efforts have been devoted to improving the morphology and developing performance of porous metal films, especially preparation of high surface area of three-dimensional porous nickel (3D-PN) films and application of their alloys in catalysis aspect and electrochemical pseudocapacitors. For example, Šimpraga et al. obtained a very high roughness factor value of the order of 2800 for Ni-Fe composite electrode prepared by simple electrochemical co-deposition process [20]. Rausch and Wendt described the high surface area sintered Ni and Raney Ni for their electrocatalytic properties [1, 21]. This mesoporous material was used as a positive electrode in hybrid supercapacitors/battery systems. Recently, the preparation of a highly porous large surface area nickel has been reported by Brown and Sotiropoulos [22]. Moreover, the nickel foam-supported porous $Ni(OH)_2$/NiOOH composite film application for

advanced pseudocapacitor material was studied by Yuan et al. [23]. However, how to control the bubble size to easily obtain attractive structure is still a great challenge.

The treatment of metal-contaminated wastewater has always been a serious issue in mining, electroplating, and the chemical and electronic industries. The impact of toxic heavy metal ions on health and on the environment has been widely reported. Metal ion treatment by adsorption into porous materials has attracted considerable attention due to their high efficiencies and economic feasibility [24, 25]. For instance, active carbon is often used to adsorb heavy metal ions and other toxic chemicals [25, 26]. Since the adsorption ability of porous materials can to a large extent be attributed to their high porosity, the adsorption ability of PN should be improved if there are suitable additives or additive combination. However, there are few studies on depollution of environment by the 3D-PN.

In electroplate industry, surfactants have been widely used as stabilizers in aqueous media to alter the surface tension of the sol/gas and protect the bubbles from coalescence. Therefore, a highly stable, well-dispersed bubble template can be obtained [27, 28]. However, there has been very little research on the effects of additive on the surface of PN film. Meanwhile, the mechanism of additive is not yet fully understood.

The research objectives of this study include first, fabricating 3D-PN film by HBDT method; second, developing 3D-network structure of PN film with the novel additive combination (PEG 10000 and 1,4-butynediol) and undertaking preliminary exploration of the impacting mechanism of additives on the morphology of PN films. In addition, the application of 3D-PN film for Zn^{2+} adsorption has been investigated in this paper, which is built upon previous respectable attempts.

2. Materials and Methods

2.1. Materials and Reagents. The electrolyte consisted of nickel sulfate, ammonium chloride, concentrated sulfuric acid, and boric acid, with the new additive combination of PEG 10000 and 1,4-butynediol. Zinc nitrate hexahydrate ($Zn(NO_3)_2{\cdot}6H_2O$) was prepared for Zn^{2+} adsorption. All the regents mentioned were of analytical grade. Cooper plate and nickel plate were purchased from Shanghai Jinan Metal Product Co., Ltd. (Shanghai, China), respectively. In the process of deposition, the solution was kept stationary. Deionized water was used throughout the experiment.

2.2. Electrode Preparation. In the study, a thin sheet of copper (99.99%) was selected for the cathode substrate material, which was repeatedly polished to highlight by numbers 400, 600, 800, and 1000 metallographic sandpaper in flowing water, cut into an area of 0.01 m × 0.05 m, and then sealed by insulating epoxy resin; only a 0.01 m × 0.01 m surface exposed to the electrolyte was kept, and a nickel plate (99.99%) with more than 0.03 m^2 acted as anode material. The distance between the two electrodes was 1 cm. Before electrodeposition, the copper substrate was dried in ovens at 150°C for 10 min, cooled to room temperature, and weighed; then the thickness of the area to be electroplated by micrometer screw was measured. And both cathode and anode were washed with deionized water in the CNC ultrasound and successively treated in the 45 g/L Na_2CO_3, 45 g/L NaOH, and 45 g/L Na_2SO_4 to remove oil; then they were immediately etched in hydrochloric acid for rough surface and then washed with deionized water. Deposition was performed in a stationary electrolyte solution (without stirring or N_2 bubbling). And it should be stressed that 3D-PN film was soaked in water for 2 min at 30°C after rinse for 1 min with deionized water. Then it was left to dry to remove residual impurities and water in constant temperature oven at 80°C for 90 min; the film was used for Zn^{2+} adsorption. All the experiments and measurements were carried out at room temperature (25 ± 1°C).

Table 1: Optimal compositions and operating conditions of the basic electrolyte.

Principal element	Optimum conditions
$NiSO_4$ (mol/L)	0.2
NH_4Cl (mol/L)	1.5
Concentrated H_2SO_4 (mL/100 mL)	0.9
H_3BO_3 (mol/L)	1.2
J_k (A/cm^2)	4.0
t (s)	25

2.3. Electrolyte and Operating Conditions Preparation. In this paper, the optimal process conditions were determined by previous experience and orthogonal test with six factors of the concentration of nickel sulfate, ammonium chloride, sulfuric acid, boric acid, cathode current density, and deposition time. In order to express easily and intuitively, the six factors above were successively referred to as C_{NiSO_4}, C_{NH_4Cl}, $C_{H_2SO_4}$, $C_{H_3BO_3}$, J_k, and t, which were generally considered to be the most important factors. Optimization of the suitable 3D-network structure can be carried out by a giant amount of research. And optimal compositions and operating conditions of the basic electrolyte were shown in Table 1. However, it was found that 3D structure of PN film was not obvious enough without additives. As shown in Table 2, different concentrations of additives (thePEG 10000 and 1,4-butynediol) were considered to be added to the electrolyte and this modificatory PN film was obtained with high specific surface area and porosity. Meanwhile, the schematic diagram of formation of PNF supported on Cu substrate was shown in Scheme 1.

2.4. Porosity and Surface Area Measurements

2.4.1. Porosity Measurements. The analytical balance was used to weigh the mass of copper substrate before deposition of the PN film and after electrodeposition process. The film was dried in oven and then reweighed. With micrometer

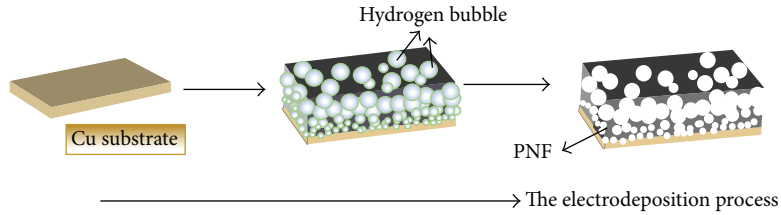

Scheme 1: A schematic diagram of formation of PNF supported on Cu substrate.

Table 2: Optimal combination and variation range of additive agent.

PEG 10000 (a) and 1, 4-butynediol (b)	Variation range (g/100 mL)	Optimal combination
Level 1	a: 0.01~0.07, b: 0	
Level 2	a: 0, b: 0.01~0.05	
Level 3	a: 0.05, b: 0.01~0.05	
Level 4	a: 0.01~0.05, b: 0.01	a: 0.03 g/100 mL, b: 0.01 g/100 mL

screw, we can determine the thickness of PN film and analyze mass variation of electrodeposition process to calculate porosity of the sample preparation. The formula was

$$\omega = \frac{\Delta m}{\rho \times \Delta h \times s}, \quad (1)$$

where Δm is the mass specimen weight (mg), ρ is the density of nickel (g/cm^3), Δh is PN film thickness (cm), and s is the contact area of the test piece and the bath (cm^2).

2.4.2. Surface Area Measurements. In the study, the A_s (specific surface area of the electrode) was performed by using electrochemical impedance spectrum (EIS) on CHI660B electrochemical workstation. Originally, the working electrode was held at −1.50 V (versus SCE) for 30 min in order to reduce the film on the electrode surface and a reproducible electrode surface could be obtained. A three-electrode test cell was used with the As-prepared PN film as working electrode, platinum foil as the counter, and a saturated calomel electrode (SCE) as the reference electrode. The sulfuric acid solution (0.5 mol/L) was used as the test solution. The EIS measurement was carried out in the frequency range from 100 kHz to 0.01 Hz under AC stimulus with 5 mV of amplitude and no applied voltage bias, which was performed on CHI660B electrochemical workstation. Subsequently, using Z-view software to fit initial EIS data, we can calculate the differential capacitance C_d. Therefore, specific surface area of the electrode is [29]:

$$A_s = \frac{C_d}{C_N A \Delta m}, \quad (2)$$

where A is the surface area of specimen and $C_N = 20\ \mu$F.

2.4.3. Environmental Applications of 3D-PN Film. Zinc nitrate solution (50 mg/L) was prepared to simulate the heavy metal ions (Zn^{2+}) in sewage. As-prepared PN film fabricated under identical optimal conditions was added into 100 mL zinc nitrate solution stirred at 120 r/min by ITCES (intelligent temperature control electromagnetic stirrer) at 25 ± 1°C. After the adsorption process, the flame atomic absorption spectrometry was used to determine the concentration of the metal ions with a standard calibration curve [30]. The mass of adsorbent could be determined by weighing the mass of cathode substrate before and after electrodeposition, respectively. Significant factors of porous nickel on the sewage purification treatment were shown in Table 3. Purification effect can be calculated by the following formulas:

Table 3: Significant factors of adsorption processes of the Zn^{2+} by the PN.

Elements	Control value
C_0C_0 ($Zn(NO)_3{\cdot}6H_2O$) (mg/L)	5
C_0 (Zn^{2+}) (mg/L)	1.099
T (min)	0.5, 2, 5, 10, 30, 40, 70, 120
m (g)	0.0083
V (L)	0.1
Temperature (°C)	25 ± 1

Note: the m is the mass of adsorbent-porous nickel by electrodeposition after 25 s under the optimal condition.

$$Q_e = \frac{V(C_0 - C_e)}{m}$$
$$Q_t = \frac{V(C_0 - C_T)}{m} \quad (3)$$
$$Q\ (\%) = \frac{(C_0 - C_e)}{C_0} \times 100\%,$$

where Q_t (mg/g), Q_e (mg/g), C_0 (mg/L), C_e (mg/L), C_T (mg/L), m (g), Q (%), and V (L) represent the adsorption capacity after a certain period of time, the equilibrium adsorption capacity, the initial concentration, adsorption equilibrium concentration of ions, concentration of ions after a certain period of time, the sorbent mass, purifying rate, and solution volume separately.

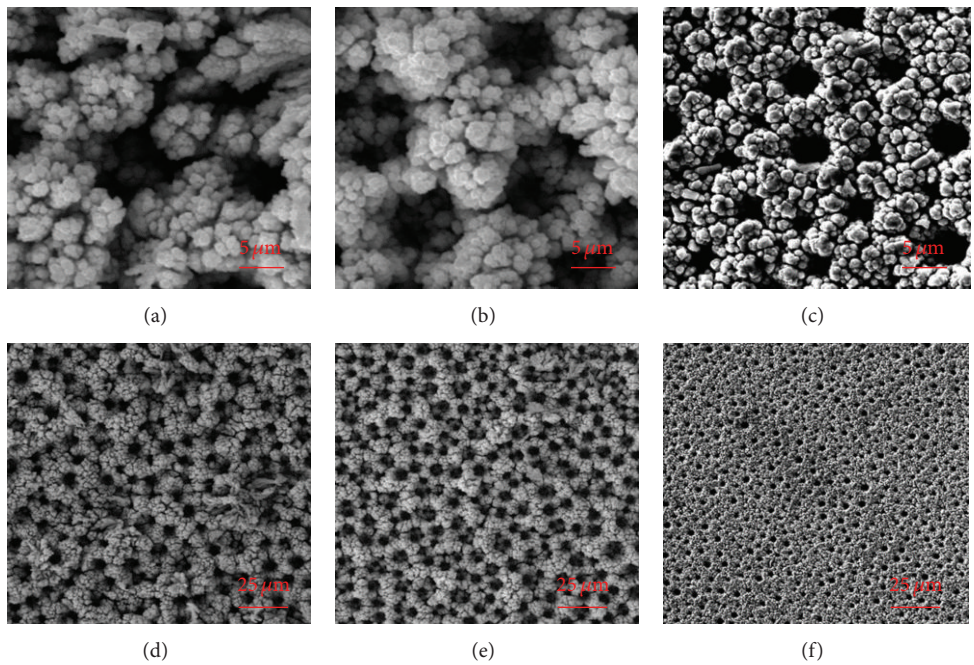

Figure 1: SEM morphology of PN film under different concentrations of PEG 10000 (0.01 (a, d), 0.05 (b, e), and 0.07 (c, f) g/100 mL).

2.4.4. SEM, XRD, and AAS Measurements. The surface morphology of as-prepared electrodes was investigated by scanning electron microscopy (SEM) (TESCAN VEGA II LMU). Crystallographic structure was studied by X-ray diffraction (XRD) using an X-ray diffraction using an automatic XRD analyzer (XRD-6000 Lab X SHIMADZU) with monochromatic Cu K_α radiation (λ = 0.15405 nm) from 10° to 80° at a speed of 4°/min. Additionally, the accelerating voltage and emission current of the XRD were, respectively, 40 kV and 30 mA. And the concentration of the zinc ion after the adsorption process was determined by atomic absorption spectrometry (AAS, 180-80 atomic absorption spectrophotometer, Hitachi, Japan) with detection wavelength of 214 nm and width of slit of 1.3 nm, respectively.

3. Results and Discussion

3.1. Effect of the PEG 10000. Figure 1 showed the surface morphology figures of PN film obtained in the electrode position of 25 s under different concentrations of PEG 10000 and fixed current density (4 A/cm^2) at the room temperature (25 ± 1°C). Meanwhile, the constituents of the electrolyte were illustrated in Table 1. And Figure 1 showed the porous structure obviously formed on the surface of the as-prepared nickel film when the concentration of the additive PEG 10000 was 0.01 g/100 mL in the electrolyte. However, the structure of hole wall of the PN film significantly changed when the concentration of that increases gradually to 0.05 g/100 mL. The diameter of main holes increased to about 10 microns and hole wall thickness decreased. Meanwhile, the grains were refined, hole density increased gradually, and surface area calculated by formula (2) also increased according to Figure 2. It should be noted that membrane structure of

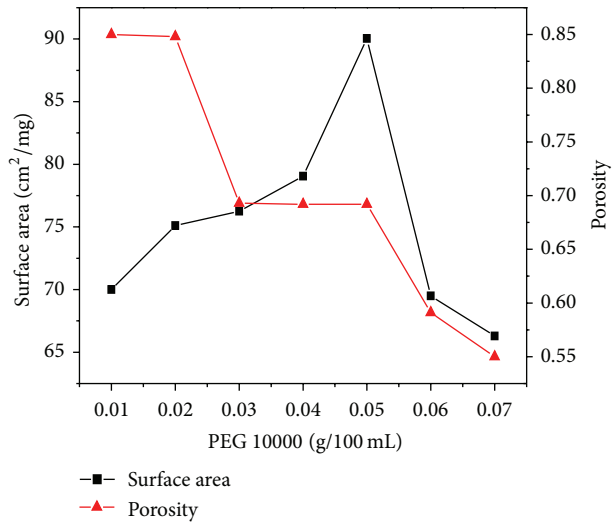

Figure 2: Effect of PEG 10000 on surface area and porosity of PN film.

the prepared PN was transformed into a 3D structure one. However, relatively more amount of additive to some extent gradually destroyed 3D structure while the concentration of PEG 10000 exceeded 0.07 g/100 mL; this could be the reason of a certain effect of nickel ions and hydrogen ions reduction reaction. And Figure 2 showed that porosity had a trend of decreasing sharply along with the increase of PEG 1000 concentration. When the amount of additive was 0.05 g/100 mL, PN film with the uniform distribution reached maximum specific surface area with relatively high porosity (Figures 1(b) and 1(e)). Therefore, the required optimization

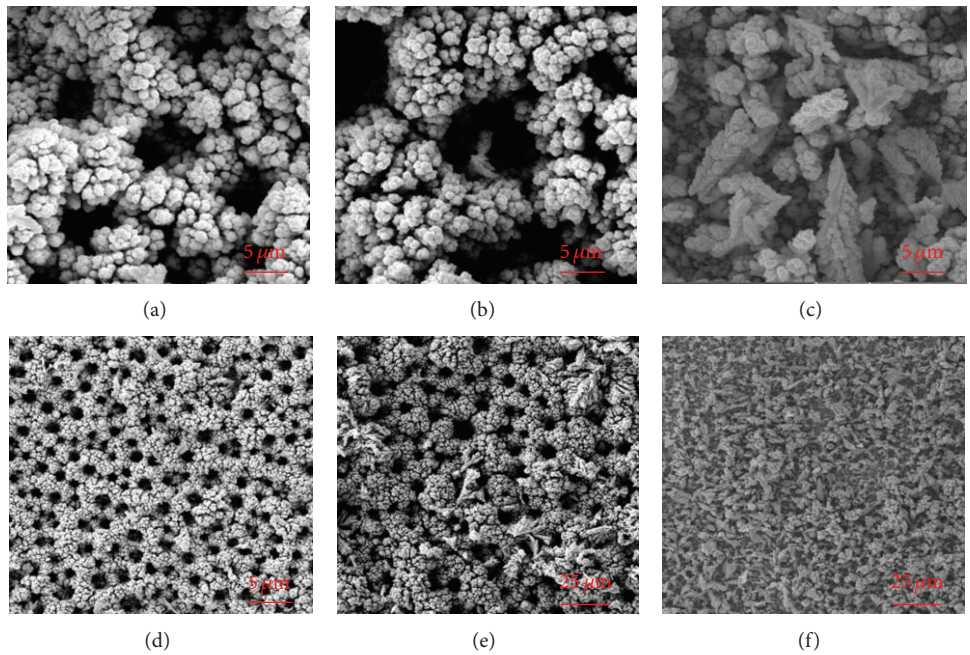

FIGURE 3: SEM morphology of PN film under different concentrations of 1,4-butynediol (0.01 (a, d), 0.03 (b, e), and 0.05 (c, f) g/100 mL).

characteristics of PN film should be prepared by controlling the amount of additive PEG 10000.

3.2. Effect of the 1,4-Butynediol. Figure 3 presented the surface morphology outline of PN film in the base plating solution of 0.2 mol/L nickel sulfate, 1.2 mol/L boric acid, 0.9 mL/100 mL concentrated sulfuric acid, and 1.5 mol/L ammonium chloride with different concentrations (0.01~0.05 g/100 mL) of 1,4-butynediol. The temperature and current density were the same as above. When adding 0.01 g/100 mL of 1,4-butynediol into electrolyte, 3D porous structure was obviously seen in Figures 3(a) and 3(d). Figure 4 showed that the porosity decreased with the concentration of 1,4-butynediol increasing (from 0.01 g/100 mL to 0.05 g/100 mL). Meanwhile, the variation tendency of porosity in Figure 4 was similar to that affected by PEG 10000 as well. However, new complex structure similar to the leaves emerged on the PN film surface with increasing concentration. Meanwhile, hole wall became thicker and sedimentary layer of dendrite coarsened. The smaller aperture was associated with the fast release rate of hydrogen bubble, resulting in an acceleration of reduction of Ni^{2+} speed-up, which also explained why dendrite of the coating coarsened. However, network structure of 3D-PN film will disappear (Figures 3(c) and 3(f)) when the concentration of additive 1,4-butynediol increases to a certain extent. Therefore, 1,4-butynediol could be also the optional additive to obtain the 3D-PN film with high surface area and appropriate porosity.

3.3. Synergy Effect of PEG 10000 and 1,4-Butynediol. Top-view SEM images of the synergy effect of 1,4-butynediol and

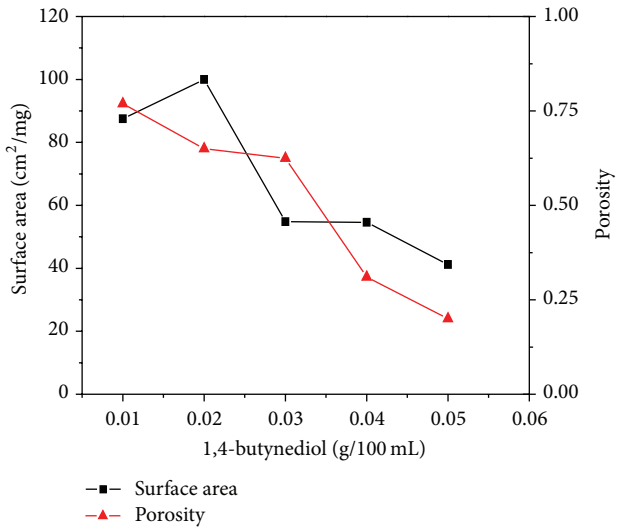

FIGURE 4: Effect of 1,4-butynediol on surface area and porosity of PN film.

PEG 10000 on PN film were shown in Figure 5. The concentration of 1,4-butynediol was controlled at 0.01 g/100 mL. With the concentration of PEG 10000 continuing to increase (from 0.01 to 0.05 g/100 mL), the hole wall of as-prepared PN film became thicker anddendrites of deposits coarsened, which was similar to the complex structure of the leaves. If the concentration of PEG 10000 was larger than 0.05 g/100 mL, a mesh and irregular structure came into being in PN film, which was largely because of some inhibitory effect of PEG 10000 on reduction reaction of nickel ions and hydrogen ions. It can be obviously seen from Figures 5(b)–5(f) that

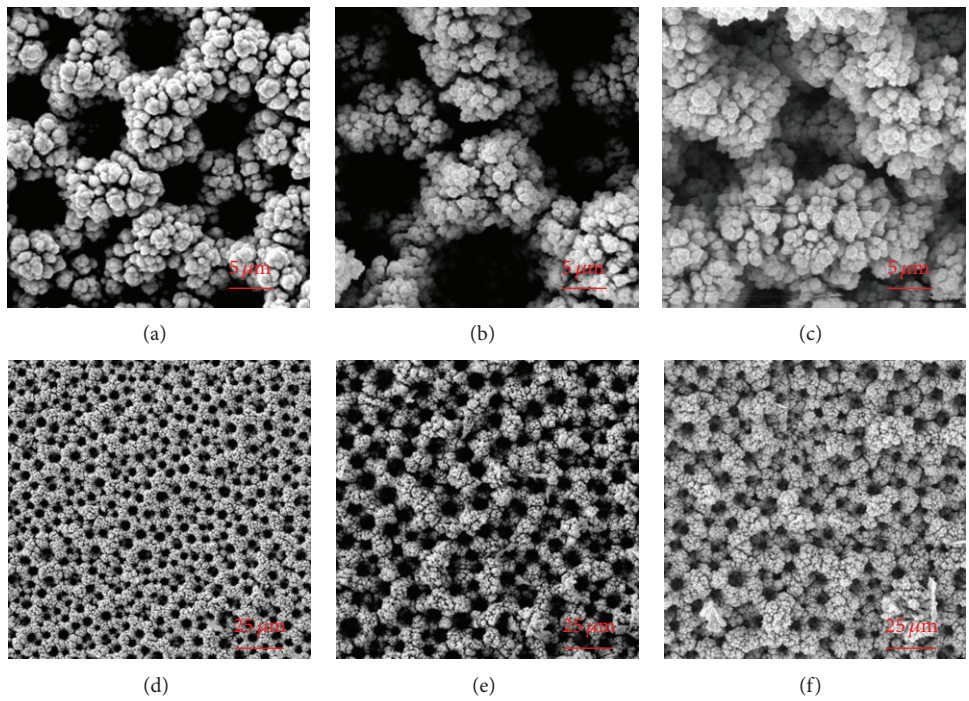

FIGURE 5: Top-view SEM images of the synergy effect of 1,4-butynediol and PEG 10000 on PN film. The concentration ratio of PEG 10000 to 1,4-butynediol is 1 : 1 (a, d), 3 : 1 (b, e), and 5 : 1 (c, f), respectively. And the concentration of 1,4-butynediol is 0.01 g/100 mL (0.01 gram of surfactant is added into 100 mL of electrolyte).

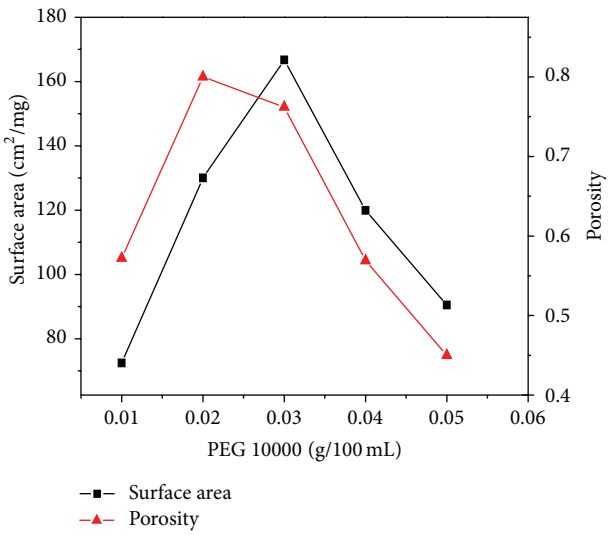

FIGURE 6: Effect of 1,4-butynediol and PEG 10000 simultaneously on PN film, and the concentration of 1,4-butynediol is controlled at 0.01 g/100 mL.

the aperture can increase to 12 microns (then decrease) and relatively homogeneous distribution. On the other hand, A_s at level 3 reached a maximum of 140.8 mg/cm^2 with sharp decline and 3D structure will be gone by continuously adding the 1,4-butynediol. The 3D-PN film with a maximum of A_s (166.7 cm^2/mg > 140.8 cm^2/mg) and porosity (0.762) was obtained when the concentration of PEG 10000 and 1,4-butynediol was 0.03 g/100 mL and 0.01 g/100 mL (Figure 6). As mentioned, tracing changes of concentration of PEG 10000 or 1,4-butylglycol could adjust and control porous structure of nickel film. And similar study about 3D porous structure with the additive was reported by Huang et al. [31]. Moreover, the more ideal 3D-PN film was fabricated by HBDT with the additive combination of PEG 10000 and 1,4-butynediol added into electrolyte. In this paper, the additive PEG 10000 with certain adsorption of metal cations [32] and good hydrophilicity because of hydrogen bond can decrease interfacial tension between the hydrogen bubble and the cathode plate (Scheme 1) and directionally align in the form of meandering structure

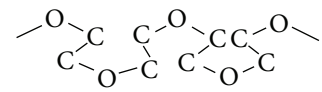

in the solution. And as a kind of gemini surfactant, the 1,4-butynediol with ideal solution interface adsorption capacity could depress rapid accumulation of hydrogen bubble (Scheme 1) and bubble size increase and largely promote the migration rate of the hydrogen bubble from cathode plate to the solution interface. Meanwhile, the additives PEG 10000 and 1,4-butynediol with a certain concentration ratio (PEG 10000: 1,4-butynediol = 3 : 1) appeared to have optimal activity to regulate the surface photography of 3D-PN film instead of mixing them together randomly. Bernardes et al. [33] observed that a cosurfactant such as decanol can induce

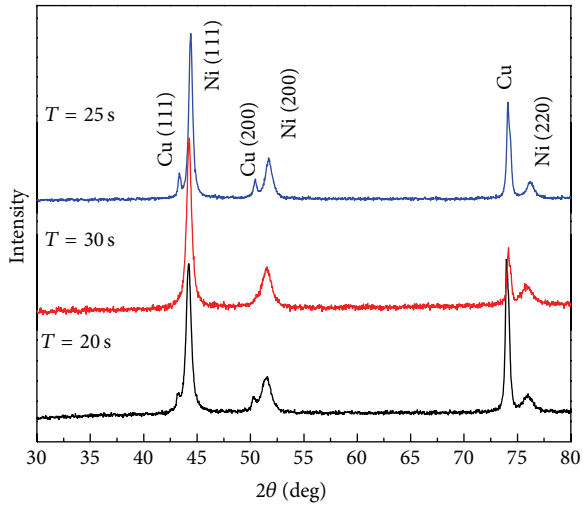

FIGURE 7: Typical XRD spectra of the PN film at different deposition times in optimized plating solution with additives (the concentration of nickel sulfate, ammonium chloride, concentrated sulfuric acid and boric acid, PEG 10000, 1,4-butynediol, cathode current density, and deposition time are 0.2 mol/L, 1.5 mol/L, 0.9 mL/100 mL, 1.2 mol/L, 0.3 g/100 mL 0.1 g/100 mL, 4.0 A/cm^2, and 25 s, resp.).

a lamellar structure. Polymer surfactant could effectively block mutual adsorption among particles, mainly relying on the solvation layer of polymer. It was worth mentioning that there was no reaction between PEG 10000 and 1,4-butynediol. Meanwhile, when the additives (PEG 10000 and 1,4-butynediol) influenced the structure of PN film simultaneously, the final effect was better than the simple individual effect, which was the key reason why the 3D structure of PN film was optimized by changing their concentrations at different levels. Therefore, the reticular 3D structure of PN film was prepared by HBDT method by controlling the concentration of the novel additive combination (Table 2).

This result was further supported by XRD spectrum. As shown in Figure 7, all of the diffraction peaks were indexed at different temperatures. The characteristics of the face-centered cubic (fcc) nickel crystal structure was evident as indicated by the orientations along the Ni (111), Ni (200), and Ni (220) directions. It was obvious that the feature peak of the copper in the X-ray diffraction pattern was caused by the copper substrate, and both the crystalline and the intensity ratios of nickel can vary with temperature. These results indicated that dentritic nickel is abundant in {111} facets. It has been known that more facets with a slower growth rate would be exposed on the crystal surface and consequently exhibit relatively stronger diffraction intensity in the corresponding XRD pattern [34]. The intensity ratio between the (111) and (200) diffraction peaks was higher than the ratio of other peaks, especially at 25°C. These strong and sharp peaks indicated that the obtained Ni crystals were highly crystalline. No detectable diffraction peaks of impurities such as copper oxide or nickel oxide signified the high purity and stability of the as-obtained products.

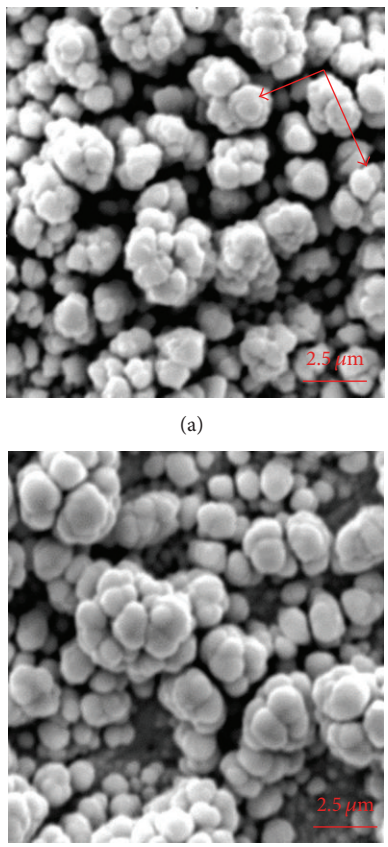

FIGURE 8: Top-view SEM images of before and after adsorption of heavy metal ions. (a) Adsorption of zinc; (b) porous nickel without zinc.

3.4. Adsorption Behavior of PN Film for Simulated Wastewater (Zn^{2+}). The PN film with high specific surface area prepared under optimal conditions exhibited certain advantages in sewage purification. Figure 8 showed surface morphology of before and after adsorption of heavy metal ions (Zn^{2+}). Compared with Figure 8(b), rough and glistening areas in the direction of arrows in Figure 8(a) were confirmed as the adsorbed Zn^{2+}. At the same time, the reliability of the zinc absorption was further demonstrated by AAS. Time-variation tendencies of Q_t and Q (%) of adsorption process of Zn^{2+} were clearly shown in Figures 9 and 10. Meanwhile, Figure 10 presented the concentration changes of Zn^{2+} during the adsorption process. The purification effect was continuously improved with the increase of time, especially in the first dozens of seconds. As time increased, the concentration of Zn^{2+} had reached equilibrium value. Meanwhile, Q_t gradually increased until maximum value (Q_e) of 9.145 mg/g for $Zn(NO_3)_2{\cdot}6H_2O$ concentrations over 5 mg/L and Q (%) 0.691, concentration of the purified sewage basically to tend stable limited to surface effective adsorption sites when the adsorption time continued to increase. The adsorption rate of PN with large specific surface area and porous structure of overlapping layers was more rapid than that of granular porous adsorbent in adsorbing heave metal

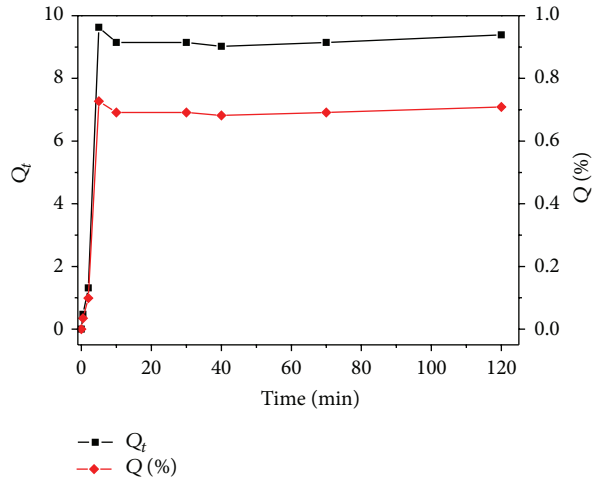

Figure 9: Effect of contact time on Q_t and Q (%) of adsorption process of zinc by PN. (conditions: volume 100 mL; temperature 25 ± 1°C; stirring speed 120 r/min).

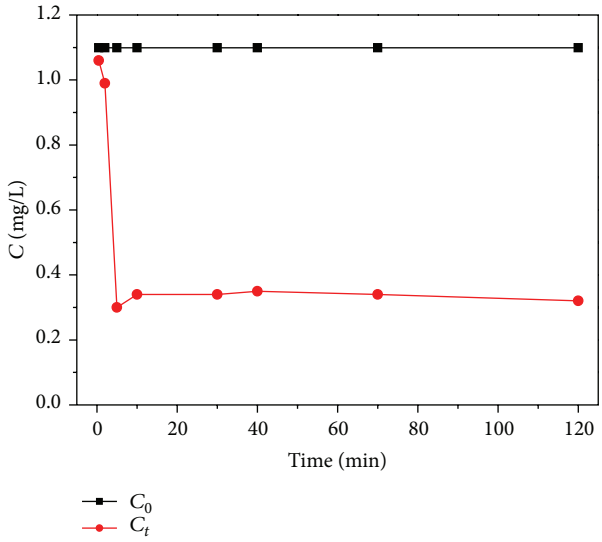

Figure 10: Concentration (C_t) changes of adsorption process of Zn^{2+} with time. (conditions: volume 100 mL; temperature 25 ± 1°C; stirring speed 120 r/min).

ions, contributing to reaching adsorption equilibrium within a short time. It is needed to be emphasized that the time elapsed for the Zn^{2+} adsorption to reach its maximum was about 10 min for the PN and there was no nickel ions in the zinc nitrate solution after adsorption equilibrium detected by AAS.

4. Conclusions

The PN film with reticular 3D network structure has been successfully fabricated by HBDT, adding novel additive combination (PEG 10000 and 1,4-butynediol) into the electrolyte. Meanwhile, the PN film with high specific surface area (A_s = 166.7 cm^2/mg) and high porosity (0.762) had open interconnected macroporous walls. The experiment conditions were optimized such that the concentration of nickel sulfate, ammonium chloride, concentrated sulfuric acid and boric acid, PEG 10000, 1,4-butynediol, cathode current density, and deposition time were 0.2 mol/L, 1.5 mol/L, 0.9 mL/100 mL, 1.2 mol/L, 0.3 g/100 mL, 0.1 g/100 mL, 4.0 A/cm^2, and 25 s, respectively, which were determined by SEM microscopic image analysis and extensive explorations. Meanwhile, the sewage (Zn^{2+}) purification of 3D-PN was investigated in this study. Adsorption capacity (Q_e and Q (%)) of PN for Zn^{2+} can reach 9.145 mg/g and 0.691 for $Zn(NO_3)_2{\cdot}6H_2O$ concentrations over 5 mg/L, which provided the possibility of the novel application of 3D-PN or other porous metals.

Conflict of Interests

The authors declare that there is no conflict of interests regarding the publication of this paper.

Acknowledgments

This work was supported by the National Natural Science Foundation of China (no. 61271059), the Natural Science Foundation Project of Chongqing (no. 2010BB4246), and the Science and Technology Development Project of Chongqing (no. CSTC2012gg-yyjs90007).

References

[1] P. A. Nelson and J. R. Owen, "A high-performance supercapacitor/battery hybrid incorporating templated mesoporous electrodes," *Journal of the Electrochemical Society*, vol. 150, no. 10, pp. A1313–A1317, 2003.

[2] H.-C. Shin and M. Liu, "Copper foam structures with highly porous nanostructured walls," *Chemistry of Materials*, vol. 16, no. 25, pp. 5460–5464, 2004.

[3] H.-C. Shin, J. Dong, and M. Liu, "Porous tin oxides prepared using an anodic oxidation process," *Advanced Materials*, vol. 16, no. 3, pp. 237–240, 2004.

[4] H.-C. Shin, J. Dong, and M. Liu, "Nanoporous structures prepared by an electrochemical deposition process," *Advanced Materials*, vol. 15, no. 19, pp. 1610–1614, 2003.

[5] K. Kusakabe, T. Kuroda, A. Murata, and S. Morooka, "Formation of a Y-type zeolite membrane on a porous α-alumina tube for gas separation," *Industrial and Engineering Chemistry Research*, vol. 36, no. 3, pp. 649–655, 1997.

[6] A. Salehi and D. Jamshidi Kalantari, "Characteristics of highly sensitive Au/porous-GaAs Schottky junctions as selective CO and NO gas sensors," *Sensors and Actuators B: Chemical*, vol. 122, no. 1, pp. 69–74, 2007.

[7] G. Zhang, C. Li, F. Cheng, and J. Chen, "$ZnFe_2O_4$ tubes: synthesis and application to gas sensors with high sensitivity and low-energy consumption," *Sensors and Actuators B: Chemical*, vol. 120, no. 2, pp. 403–410, 2007.

[8] L. Wang, H. W. Xu, P. C. Chen, D. W. Zhang, C. X. Ding, and C. H. Chen, "Electrostatic spray deposition of porous Fe_2O_3 thin films as anode material with improved electrochemical performance for lithium-ion batteries," *Journal of Power Sources*, vol. 193, no. 2, pp. 846–850, 2009.

[9] L. Yuan, Z. P. Guo, K. Konstantinov, H. K. Liu, and S. X. Dou, "Nano-structured spherical porous SnO_2 anodes for lithium-ion batteries," *Journal of Power Sources*, vol. 159, no. 1, pp. 345–348, 2006.

[10] J.-Y. Li, S. Xiong, J. Pan, and Y. Qian, "Hydrothermal synthesis and electrochemical properties of urchin-like core-shell copper oxide nanostructures," *Journal of Physical Chemistry C*, vol. 114, no. 21, pp. 9645–9650, 2010.

[11] N. Kanetake and M. Kobashi, "Innovative processing of porous and cellular materials by chemical reaction," *Scripta Materialia*, vol. 54, no. 4, pp. 521–525, 2006.

[12] Y.-S. Hu, Y.-G. Guo, W. Sigle, S. Hore, P. Balaya, and J. Maier, "Electrochemical lithiation synthesis of nanoporous materials with superior catalytic and capacitive activity," *Nature Materials*, vol. 5, no. 9, pp. 713–717, 2006.

[13] G. X. Pan, X. Xia, F. Cao, P. S. Tang, and H. F. Chen, "Porous $Co(OH)_2$/Ni composite nanoflake array for high performance supercapacitors," *Electrochimica Acta*, vol. 63, pp. 335–340, 2012.

[14] Y. Guo, H. Yui, H. Minamikawa et al., "Dimension control of glycolipid nanotubes by successive use of vesicle extrusion and porous template," *Chemistry of Materials*, vol. 18, no. 6, pp. 1577–1580, 2006.

[15] I. Kazeminezhad, A. C. Barnes, J. D. Holbrey, K. R. Seddon, and W. Schwarzacher, "Templated electrodeposition of silver nanowires in a nanoporous polycarbonate membrane from a nonaqueous ionic liquid electrolyte," *Applied Physics A: Materials Science and Processing*, vol. 86, no. 3, pp. 373–375, 2007.

[16] J. H. Yuan, F. Y. He, D. C. Sun, and X. H. Xia, "A simple method for preparation of through-hole porous anodic alumina membrane," *Chemistry of Materials*, vol. 16, no. 10, pp. 1841–1844, 2004.

[17] W. Chen, J.-H. Yuan, and X.-H. Xia, "Characterization and manipulation of the electroosmotic flow in porous anodic alumina membranes," *Analytical Chemistry*, vol. 77, no. 24, pp. 8102–8108, 2005.

[18] F. C. Meldrum and R. Seshadri, "Porous gold structures through templating by echinoid skeletal plates," *Chemical Communications*, no. 1, pp. 29–30, 2000.

[19] D. D. Krassimir, D. S. Valkovska, and P. A. Kralchevsky, "Hydrodynamic instability and coalescence in trains of emulsion drops or gas bubbles moving through a narrow capillary," *Journal of Colloid and Interface Science*, vol. 267, no. 1, pp. 243–258, 2003.

[20] R. Šimpraga, G. Tremiliosi-Filho, S. Y. Qian, and B. E. Conway, "In situ determination of the "real area factor" in H_2 evolution electrocatalysis at porous Ni-Fe composite electrodes," *Journal of Electroanalytical Chemistry*, vol. 424, no. 1-2, pp. 141–151, 1997.

[21] S. Rausch and H. Wendt, "Morphology and utilization of smooth hydrogen-evolving raney nickel cathode coatings and porous sintered-nickel cathodes," *Journal of the Electrochemical Society*, vol. 143, no. 9, pp. 2852–2862, 1996.

[22] I. J. Brown and S. Sotiropoulos, "Electrodeposition of Ni from a high internal phase emulsion (HIPE) template," *Electrochimica Acta*, vol. 46, no. 17, pp. 2711–2720, 2001.

[23] Y. F. Yuan, X. H. Xia, J. B. Wu, J. L. Yang, Y. B. Chen, and S. Y. Guo, "Nickel foam-supported porous $Ni(OH)_2$/NiOOH composite film as advanced pseudocapacitor material," *Electrochimica Acta*, vol. 56, no. 6, pp. 2627–2632, 2011.

[24] W. S. W. Ngah and M. A. K. M. Hanafiah, "Biosorption of copper ions from dilute aqueous solutions on base treatedrubber (Hevea brasiliensis) leaves powder: kinetics, isotherm, and biosorption mechanisms," *Journal of Environmental Sciences*, vol. 20, no. 10, pp. 1168–1176, 2008.

[25] N. Zhang, H. Qiu, Y. Si, W. Wang, and J. Gao, "Fabrication of highly porous biodegradable monoliths strengthened by graphene oxide and their adsorption of metal ions," *Carbon*, vol. 49, no. 3, pp. 827–837, 2011.

[26] S. Babel and T. A. Kurniawan, "Low-cost adsorbents for heavy metals uptake from contaminated water: a review," *Journal of Hazardous Materials*, vol. 97, no. 1–3, pp. 219–243, 2003.

[27] L. Wang and R.-H. Yoon, "Role of hydrophobic force in the thinning of foam films containing a nonionic surfactant," *Colloids and Surfaces A: Physicochemical and Engineering Aspects*, vol. 282-283, pp. 84–91, 2006.

[28] F. Melo and J. S. Laskowski, "Fundamental properties of flotation frothers and their effect on flotation," *Minerals Engineering*, vol. 19, no. 6-8, pp. 766–773, 2006.

[29] X. S. Dong, J. Q. Jiang, and T. Tian, "Effect of process parameters on specific surface area of porous nickel film obtained by electrodeposition with hydrogen bubbles as template," *Electroplating & Finishing*, vol. 30, no. 2, pp. 1–3, 2011.

[30] I. S. I. Adam and A. N. Anthemidis, "Flow injection wetting-film extraction system for flame atomic absorption spectrometric determination of cadmium in environmental waters," *Talanta*, vol. 77, no. 3, pp. 1160–1164, 2009.

[31] L. Huang, H.-B. Wei, F.-S. Ke, X.-Y. Fan, J.-T. Li, and S.-G. Sun, "Electrodeposition and lithium storage performance of three-dimensional porous reticular Sn-Ni alloy electrodes," *Electrochimica Acta*, vol. 54, no. 10, pp. 2693–2698, 2009.

[32] H. J. Sun, H. B. Jiang, S. H. Li et al., "Effect of alcohols as additives on the performance of a nano-sized Ru-Zn(2.8%) catalyst for selective hydrogenation of benzene to cyclohexene," *Chemical Engineering Journal*, vol. 218, pp. 415–424, 2003.

[33] J. S. Bernardes, J. Norrman, L. Piculell, and W. Loh, "Complex polyion-surfactant ion salts in equilibrium with water: changing aggregate shape and size by adding oil," *Journal of Physical Chemistry B*, vol. 110, no. 46, pp. 23433–23442, 2006.

[34] Y. Xiong and Y. Xia, "Shape-controlled synthesis of metal nanostructures: the case of palladium," *Advanced Materials*, vol. 19, no. 20, pp. 3385–3391, 2007.